# Cooperative vibronic transitions in $Eu^{3+}$-doped oxide glasses

Masanori Tanaka
*Single Quantum Dot Project, ERATO, Japan Science and Technology Corporation (JST), Satellite-2, Tsukuba Research Consortium 5-9-9 Tokodai, Tsukuba, Ibaraki 300-2635, Japan*

Takashi Kushida
*Graduate School of Materials Science, Nara Institute of Science and Technology, Ikoma, Nara 630-0101, Japan*
(Received 12 July 1999)

The vibronic spectra involving intramolecular vibrations of glass forming units have been measured for the $^7F_0$-$^5D_J$ ($J=0,1,2,4$) and $^7F_1$-$^5D_1$ transitions of the $Eu^{3+}$ ion in four kinds of oxide glasses: $Ca(PO_3)_2$, $SiO_2$-$Na_2O$, $GeO_2$-$Na_2O$, and $TeO_2$-$Na_2O$. The relative intensities of these spectra are analyzed quantitatively on the basis of the cooperative optical transition model proposed by Stavola and Dexter, which assumes that the $f$-$f$ vibronic transition is allowed by the electrostatic interaction between the rare-earth ion and an oscillating ligand molecule. The fact that the vibronic spectra of the $^7F_0$-$^5D_2$ and $^7F_1$-$^5D_1$ transitions are fairly intense compared with the others is shown to be explained well by this model, because these spectra are predicted to occur through the electric dipole-dipole interaction which is the most dominant among the multipole expansion terms of the above electrostatic interaction. The principal mechanisms of the $^7F_0$-$^5D_0$ and $^7F_0$-$^5D_1$ vibronic transitions are identified as due to the borrowing of intensities from the $^7F_2$-$^5D_0$ and $^7F_2$-$^5D_1$ vibronic transitions respectively, which are predicted to be caused by the dipole-dipole coupling in the above model, via the mixing of the $^7F_2$ manifold into $^7F_0$ through the second-order component of the crystal-field potential. In addition, the vibronic spectrum of the $^7F_0$-$^5D_4$ transition is ascribed to the mechanism through the electric octopole-dipole coupling and possibly also to the crystal-field mixing effect for the $^5D_4$ manifold. These results show that the interaction of the $Eu^{3+}$ ion with the vibrations of the surrounding forming units of oxide glasses is described well by the electric multipole-multipole interaction.
[S0163-1829(99)00646-3]

## I. INTRODUCTION

Recently, rare-earth-doped glasses have attracted much interest from the viewpoint of practical applications to optical fiber amplifiers,[1] wavelength-selective optical memories,[2] up-conversion emission materials,[3] and so on. The properties of these optical devices are affected largely by various processes caused by the interaction between the rare-earth ion and the vibrations of the host, such as nonradiative deexcitation, spectral line broadening due to dephasing, and phonon-assisted energy transfer. Accordingly, the studies of this interaction are very important for the development of materials for these applications. Since vibronic spectra reflect the electron-vibration coupling strength and also the density of states of vibrational modes, we can obtain significant information on the interaction between the optically active ion and the vibrations from the investigation of these spectra.

The Franck-Condon mechanism[4] is generally not important in the vibronic spectrum of the $f$-$f$ transition of rare-earth ions in condensed matter.[5–12] This is because the $4f$ electron-phonon (or vibration) interaction is very weak on account of the shielding of the $4f$ electrons from the surroundings by outer $5s^2$ and $5p^6$ electrons. Therefore, the equilibrium configuration of the nucleus system can be regarded to be independent of the $4f^N$ electronic state of the rare-earth ion. Namely, the Haung-Rhys factor is almost zero and the vibronic transition due to the Franck-Condon mechanism is usually negligible, although some exceptions have been reported.[13,14] There exist two representative theorerical approaches, which were proposed by Faulkner and Richardson[7,8] and by Stavola and Dexter,[11,12] for vibronic spectra of the $f$-$f$ transition of rare-earth ions. The natures of the vibrations which were treated in these approaches are different. The vibronic transition caused through the vibrational modes of the rare-earth ion-ligand system was discussed in the former on the basis of the Herzberg-Teller mechanism. In the latter approach, on the other hand, the vibronic spectra involving intramolecular vibrations of the ligand were treated as due to the cooperative optical transition processes in which the rare-earth electronic and intramolecular vibrational transitions occur simultaneously through the electrostatic interaction between the rare-earth ion and the oscillating ligand molecule.

In this paper, we investigate the vibronic spectra which accompany the $^7F_0$-$^5D_J$ ($J=0,1,2,4$) and $^7F_1$-$^5D_1$ transitions of the $Eu^{3+}$ ion ($4f^6$) in various kinds of oxide glasses [calcium metaphosphateglass, sodium silicate glass, sodium germanate glass, and sodium tellurite glass]. (See Fig. 1 for the energy level diagram of the $Eu^{3+}$ ion.) Since the observed vibronic spectra involve the intramolecular vibrations of the glass forming units,[15,16] such as $SiO_4$ tetrahedra in sodium silicate glass,[17,18] we analyze these intensities quantitatively by means of the cooperative optical transition model of Stavola and Dexter.[11,12]

The vibronic spectra of the $^7F_0$-$^5D_0$ and $^7F_0$-$^5D_1$ transitions are forbidden by the Stavola-Dexter theory, when the static crystal-field potential acting on the rare-earth ion is not taken into account. However, they are observed in our

 

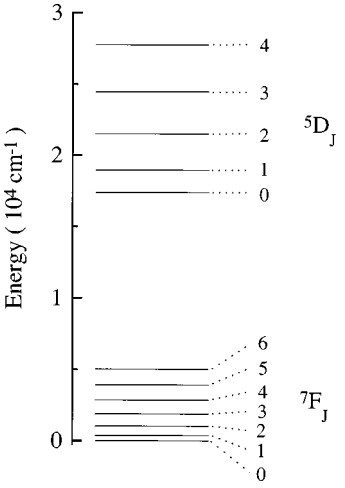


FIG. 1. The energy level scheme due to the $4f^6$ electron configuration of the $Eu^{3+}$ ion. The numbers in the scheme denote the inner quantum numbers $J$ of the $^7F_J$ and $^5D_J$ multiplets. The $^5L_J$ and $^5G_J$ multiplets, which exist between the $^5D_3$ and $^5D_4$ states, are omitted for simplicity.

samples. It has been proved by our group[19] that the crystal-field-induced mixing between the $4f^6$ states ($J$ mixing) contributes dominantly to the fluorescence intensity and the inhomogeneous broadening of the purely electronic $^5D_0$-$^7F_0$ transition of $Eu^{3+}$ in oxide glasses.[19] Further, we have recently shown that the homogeneous spectral width of this transition in glasses can be explained well by the two-phonon Raman scattering or the interaction between the rare-earth ion and the flipping two-level systems if we take into account the $J$ mixing.[20] In this paper, we also examine the possibility that the above two forbidden vibronic spectra are explained by $J$ mixing. A part of the present results has already been reported briefly.[21,22]

## II. THEORY

### A. Summary of the cooperative optical transition model

In this subsection, we summarize the theory of the cooperative optical transition developed by Stavola and Dexter[11,12] for the vibronic spectra of the $f$-$f$ transition of a rare-earth ion. In this approach, the electrostatic interaction between the rare-earth ion and an oscillating ligand molecule is taken into account as a perturbation for the ion-molecule system up to the first order, and this interaction is assumed to allow the electric-dipole vibronic transition involving the $f$-$f$ transition of the rare-earth ion and the excitation or dexcitation of the intramolecular vibration of the ligand molecule. The above authors neglected the overlap of the charge distributions localized on the rare-earth ion and the ligand, and expressed the electrostatic interaction in terms of a series of multipole-multipole expansion. They adopted the intermediate coupled states $|4f^N[\alpha SL]J\rangle$ of the free ion as the initial and final states of the transition of the rare-earth ion. Here, square brackets denote that the quantities in the parentheses are not good quantum numbers, and $\alpha$ is additional quantum numbers to define the energy level uniquely. Further, they employed the closure approximation of Judd[23] and Ofelt[24] for the high-lying $4f^{N-1}nl$ configuration states of the rare-earth ion which admix into the $4f^N$ states through the above interaction. As a result, the squared absolute value of the transition matrix element for the $|4f^N[\alpha SL]J\rangle \rightarrow |4f^N[\alpha' S' L']J'\rangle$ vibronic transition acompanied by the excitation of a strongly infrared-active intramolecular vibration is calculated as

$$\frac{1}{2J+1}\sum_{k_1}\sum_{\lambda=2,4,6}\frac{1}{\kappa^2}\left(\frac{e^2}{R^{k_1+2}}\right)^2(2\lambda+1)\frac{k_1+1}{3}\Xi(k_1,\lambda)^2 \times|\langle 4f^N[\alpha' S' L']J'\|\mathbf{U}^{(\lambda)}\|4f^N[\alpha SL]J\rangle|^2 \times|\langle g1|\mathbf{M}_{\mathrm{m}}^{(1)}|g0\rangle|^2 \quad (1)$$

with

$$\Xi(k_1,\lambda)=2\sum_{nl}\begin{Bmatrix}1 & \lambda & k_1\\ f & l & f\end{Bmatrix}\langle 4f|r|nl\rangle\langle 4f|r^{k_1}|nl\rangle \times\langle f\|\mathbf{C}^{(1)}\|l\rangle\langle l\|\mathbf{C}^{(k_1)}\|f\rangle/\Delta(nl). \quad (2)$$

Here, the dependence on the orientation of the ligand molecule relative to the rare-earth ion is averaged out, all the components $|4f^N[\alpha SL]JM_J\rangle$ $(M_J=-J,-J+1,\ldots,J-1,J)$ of the initial-state manifold of the rare-earth ion are assumed to be equally populated, and only the electric dipole with the moment $\mathbf{M}_{\mathrm{m}}^{(1)}$ is considered as the multipole of the ligand molecule. Further, $k_1$ is the index of the electric $2^{k_1}$ pole of a rare-earth ion, which appears from the multipole expansion of the electrostatic interaction of the ion with the oscillating molecule, and $\langle\cdots\|\mathbf{U}^{(\lambda)}\|\cdots\rangle$ is the reduced matrix element of the unit tensor operator $\mathbf{U}^{(\lambda)}$ of rank $\lambda$. The electron charge, the dielectric constant, and the separation between the centers of gravity of the rare-earth ion and the molecule are denoted as $-e$, $\kappa$, and $R$, respectively. $|g0\rangle$ and $|g1\rangle$ represent that the intramolecular vibrational quantum numbers are 0 and 1, respectively, in the electronic ground state of the ligand molecule. $\Delta(nl)$ is the representative energy separation between the $4f^{N-1}nl$ and $4f^N$ configuration states. Furthermore, $\langle 4f|r^{k_1}|nl\rangle$ and $\langle l\|\mathbf{C}^{(k_1)}\|f\rangle$ are defined, respectively, as follows:

$$\langle 4f|r^{k_1}|nl\rangle=\int_0^\infty \chi_{4f}(r)r^{k_1}\chi_{nl}(r)dr \quad (3)$$

and

$$\langle l\|\mathbf{C}^{(k_1)}\|f\rangle=(-1)^l\sqrt{7(2l+1)}\begin{pmatrix}l & k_1 & 3\\ 0 & 0 & 0\end{pmatrix}. \quad (4)$$

Here, $\chi_{nl}(r)/r$ is the radial part of the appropriate single $nl$-electron wave function. The selection rule for $J$ of the vibronic transition is obtained from the reduced matrix element of $\mathbf{U}^{(\lambda)}$ in expression (1) and the 6-$j$ symbol in expression (2) as

$$|J-J'|\leq\lambda\leq J+J' \quad (\lambda=2,4,6). \quad (5)$$

In addition, the 6-$j$ symbol and two 3-$j$ symbols contained in $\langle l\|\mathbf{C}^{(k_1)}\|f\rangle$ and $\langle f\|\mathbf{C}^{(1)}\|l\rangle$ of Eq. (2) require that $\lambda$ and $k_1$ satisfy the relation

$$|\lambda-k_1|\leq 1 \quad (k_1=1,3,5,7) \quad (6)$$

and also that $l=d$, $g$. The two conditions (5) and (6) predict that the vibronic spectra of the $^7F_0$-$^5D_2$ and $^7F_1$-$^5D_1$ transitions are caused through the electric dipole-dipole and octopole-dipole interactions between the rare-earth ion and a ligand molecule, while that of the $^7F_0$-$^5D_4$ transition is done through the electric octopole-dipole and $2^5$-pole-dipole interactions.

Here, we make a comparison of the cooperative optical transition model with Faulkner and Richardson's theory.[7,8] These authors considered that the dynamical component of the electrostatic interaction between the rare-earth ion and the ligands due to vibrations of the rare-earth ion-ligand system as a perturbation, and assumed that the displacement-dependent electrostatic interaction at the rare-earth ion site allows the vibronic spectrum of the $f$-$f$ transition. In this approach, the symmetry of the vibrational mode must satisfy a condition which is resrticted by the point symmetry of the static crystal-field potential, and this gives a selection rule of the vibronic transition. This point is in contrast to the cooperative transition model which does not require such a condition. As a simple example, let us consider the system in which the rare-earth ion lies at the centrosymmetric site. In this case, the treatment of Faulkner and Richardson requires the participation of an odd-parity vibrational mode, which removes inversion symmetry of the static crystal-field, for the $f$-$f$ vibronic transition to take place, while the electric dipole vibronic transition in the cooperative transition model can occur irrespectively of whether the intramolecular vibration concerned induces noncentrosymmetry at the ion site or not.

### B. $J$-mixing effect on the vibronic spectra of the $^7F_0$-$^5D_J$ ($J=0,1,4$) transitions

Since the $^7F_0$-$^5D_0$ and $^7F_0$-$^5D_1$ vibronic transitions do not satisfy the selection rule (5), the theory of Stavola and Dexter predicts zero intensities for these transitions. However, these vibronic spectra are observed in the $Eu^{3+}$-doped oxide glasses. The $J$-mixing effect caused by the even-parity crystal-field components is a possible mechanism which accounts for these spectra on the basis of the cooperative transition model.

Now, let us consider the contribution of the $J$ mixing to the vibronic spectra of the $^7F_0$-$^5D_0$ and $^7F_0$-$^5D_1$ transitions. The $J$ mixing between the $^5D_J$ manifolds is not considered to be as effective as that between the $^7F_J$ manifolds, because the energy separations between the $^5D_J$ manifolds are larger than those between the $^7F_J$ manifolds and also because the absolute value of the reduced matrix element $\langle 4f^6[^5D]_J\|\mathbf{U}^{(\lambda)}\|4f^6[^5D]_0\rangle$ is smaller than that of $\langle 4f^6[^7F]_J\|\mathbf{U}^{(\lambda)}\|4f^6[^7F]_0\rangle$. Therefore, we neglect the $J$-mixing effect for the $^5D_0$ and $^5D_1$ states. The $^7F_{2,4,6}$ manifolds mix into the $^7F_0$ state through the even-parity crystal-field perturbation. However, because the $^7F_2$ manifold is the closest in energy to the $^7F_0$ state among the three manifolds, here we consider only the mixture of $^7F_2$ into $^7F_0$.

We express the static crystal-field potential acting on the $Eu^{3+}$ ion as

$$V_c=\sum_k V_c^{(k)}=\sum_{k,q}\sum_i B_{kq}C_q^k(\theta_i,\phi_i), \tag{7}$$

with

$$C_q^{(k)}(\theta_i,\phi_i)=\sqrt{\frac{4\pi}{2k+1}}Y_{kq}(\theta_i,\phi_i),$$

where $(r_j,\ \theta_j,\ \phi_j)$ is the position of the $j$th $4f$ electron of the $Eu^{3+}$ ion, $Y_{kq}(\theta_i,\phi_i)$ is the $q$ component of the $k$th-order spherical harmonics, and $B_{kq}$ is the $k$th-order crystal-field parameter. Then, the wave function of the $^7F_0$ state with the mixture of $^7F_2$ is written by the first-order perturbation theory as

$$|4f^6[^7F_0]\rangle=|4f^6[^7F]_0\rangle-\frac{2\sqrt{3}}{15\Delta_{20}}\times\sum_{q=-2}^{2}(-1)^qB_{2q}|4f^6[^7F]_2M_J=q\rangle, \tag{8}$$

where $\Delta_{20}$ is the energy separation between the free-ion $^7F_2$ and $^7F_0$ states. By using Eq. (8), the transition matrix elements in the cooperative transition model for the vibronic spectra of the $^7F_0$-$^5D_{J'}(J'=0,1)$ transitions are expressed as

$$\langle 4f^6[^5D]_{J'}M_{J'},g1|\boldsymbol{\mu}|4f^6[^7F_0],g0\rangle_{ct}=-\frac{2\sqrt{3}}{15\Delta_{20}}\sum_{q=-2}^{2}(-1)^qB_{2q}\times\langle 4f^6[^5D]_{J'}M_{J'},g1|\boldsymbol{\mu}|4f^6[^7F]_2M_J=q,g0\rangle_{ct}. \tag{9}$$

Here, $\boldsymbol{\mu}$ is the electric dipole moment of the $Eu^{3+}$-ligand molecule system, and the suffix ct denotes that the transition matrix element is based on the cooperative transition model. This expression means that the vibronic spectra of the $^7F_0$-$^5D_0$ and $^7F_0$-$^5D_1$ transitions can obtain intensities, if the second-order crystal-field component $V_c^{(2)}$ exists, from those of the $^7F_2$-$^5D_0$ and $^7F_2$-$^5D_1$ transitions, respectively, which are permitted to occur through the dipole-dipole interaction between the $Eu^{3+}$ ion and the ligand molecule.

Two types of mechanisms are able to account for the $^7F_0$-$^5D_4$ vibronic transition. One is the cooperative transition process through the electric octopole-dipole coupling mentioned above. The other is due to the $J$ mixing. Similarly as in the case of the $^7F_0$-$^5D_0$ and $^7F_0$-$^5D_1$ vibronic transitions, the mixing of the $^7F_2$ state into $^7F_0$ makes it possible for the vibronic spectrum of the $^7F_0$-$^5D_4$ transition to borrow intensity from the vibronic spectrum of the $^7F_2$-$^5D_4$ transiton, which satisfies the conditions for the vibronic transition caused by the electric dipole-dipole interaction in the expressions (5) and (6). If this wave-function mixing plays the dominant role in the intensity of the $^7F_0$-$^5D_4$ vibronic transition, the transition matrix element for this vibronic spectrum is described by Eq. (9) with $J'=4$. Further, we consider the $J$ mixing for the $^5D_4$ state. The $^5G_J$ and $^5L_J$ manifolds lie in the vicinity of the $^5D_4$ state in energy, and these manifolds admix into the $^5D_4$ state by the even-parity crystal-field potential. Thus, the $^7F_0$-$^5D_4$ vibronic transition

can obtain intensities from the $^7F_0$-$^5G_{2,4,6}$ and $^5L_6$ vibronic transitions which are permitted by the selection rules (5) and (6).

### III. EXPERIMENTAL PROCEDURES

The samples used in this study were four kinds of $Eu^{3+}$-doped oxide glasses; calcium metaphosphate glass $[(76)Ca(PO_3)_2(24)Eu_2O_3]$, sodium silicate glass $[(70)SiO_2(30)Na_2O(1)Eu_2O_3]$, sodium germanate glass $[(80)GeO_2(20)Na_2O(1)Eu_2O_3]$, and sodium tellurite glass $[(80)TeO_2(20)Na_2O(1)Eu_2O_3]$. Here, the numbers in the parentheses denote the mole ratios of the components. Hereafter, these samples are denoted as $Ca(PO_3)_2$, $SiO_2$-$Na_2O$, $GeO_2$-$Na_2O$, and $TeO_2$-$Na_2O$ glasses, respectively.

The fluorescence excitation spectra were measured for these samples at room temperature and 2 K. The excitation beam in the 17 000–30 000 $cm^{-1}$ wave number range was obtained by passing the light of a tungsten halogen lamp or a Xe lamp through a monochromator (Chromatix CT 103). The most intense $^5D_0$-$^7F_2$ fluorescence was monitored using a monochromator (Nikon P250) equipped with a cooled photomultiplier (Hamamatsu R-928).

The correction for the wavelength dependence of the excitation light intensity was made by using a rhodamine B-ethylene glycol solution [3$g$/l], whose quantum efficiency is known to be constant in the 240–590 nm wavelength range.

The fluorescence spectra due to the $^5D_{2,1,0}$-$^7F_J$ transitions were also measured at room temperature and 77 K for all the samples under the excitation of the 465.8 nm line of an $Ar^+$ laser (Spectra Physics model 2016). The fluorescence through a double monochromator (Spex 14018) was detected by a cooled photomultiplier (Hamamatsu R-928). Furthermore, the $^5D_0$-$^7F_1$ fluorescence spectrum was measured at 77 K under the site-selective $^7F_0$-$^5D_0$ excitation with a cw rhodamine-6G dye laser pumped by all lines of an $Ar^+$ laser (Spectra Physics model 2016).

### IV. EXPERIMENTAL RESULTS

Figure 2 shows the excitation spectra of fluorescence at room temperature for the above-mentioned four kinds of oxide glasses. The small peak in the higher energy side of the $^7F_0$-$^5D_1$ zero-phonon line is not assigned to the vibronic spectrum of the $^7F_0$-$^5D_1$ transition but to that of the $^7F_1$-$^5D_1$ transition for all the samples. The vibronic spectrum of the $^7F_0$-$^5D_4$ transition was observed for $SiO_2$-$Na_2O$ (see Fig. 3) and $GeO_2$-$Na_2O$ glasses, but was not detectable for the other samples on account of its very weak intensity and the overlapping of the inhomogeneously broadened $^7F_0$-$^5D_4$ electronic transition. The vibronic spectra of the $^7F_0$-$^5D_1$ and $^7F_0$-$^5D_0$ transitions are not seen in Figs. 2(a)–2(d), because the $^7F_2$-$^5D_2$ and $^7F_2$-$^5D_1$ zero phonon spectra, which are due to the absorption from the thermally excited states, overlap with the $^7F_0$-$^5D_1$ and $^7F_0$-$^5D_0$ vibronic transitions, respectively. [The bands peaked at about 20550 and 18100 $cm^{-1}$ in Figs. 2(a)–2(d) are due to the $^7F_2$-$^5D_2$ and $^7F_2$-$^5D_1$ zero phonon spectra, respectively.]

Figure 4 shows the excitation spectrum of fluorescence at 2 K in the $GeO_2$-$Na_2O$ glass. As a result of the disappearance of the above excited-state absorption, the vibronic spectra of the $^7F_0$-$^5D_0$ and $^7F_0$-$^5D_1$ transitions are observed.

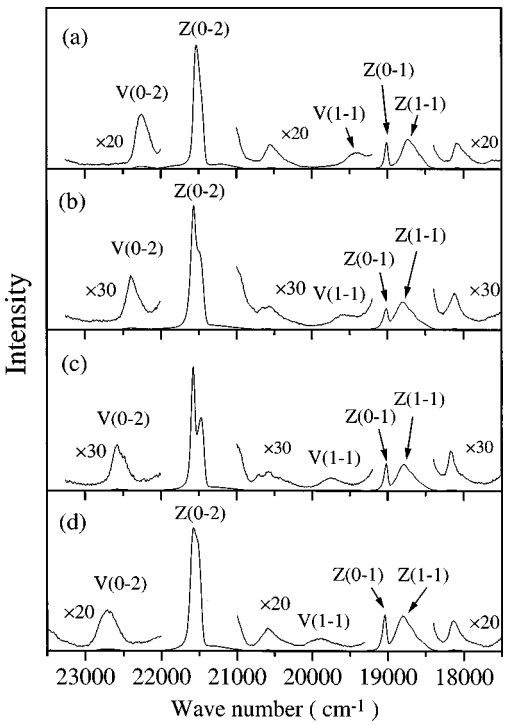


FIG. 2. Fluorescence excitation spectra of the $Eu^{3+}$ ion doped into (a) $TeO_2$-$Na_2O$, (b) $GeO_2$-$Na_2O$, (c) $SiO_2$-$Na_2O$, and (d) $Ca(PO_3)_2$ glasses, at room temperature. $Z(J\text{-}J')$ and $V(J\text{-}J')$ denote the zero-phonon line and the vibronic spectrum of the $^7F_J$-$^5D_{J'}$ transition, respectively.

### V. ANALYSIS AND DISCUSSION

Figure 5 shows the fluorescence spectra of our four glass samples at 77 K. In all the samples, the fluorescence intensities due to the $^5D_{1,2}$-$^7F_J$ transitions are much weaker than those due to the $^5D_0$-$^7F_J$ transitions. This indicates that the nonradiative relaxation rate from the $^5D_{1,2}$ states to $^5D_0$ is considerably high in the $Eu^{3+}$ ions. From the theoretical ex-

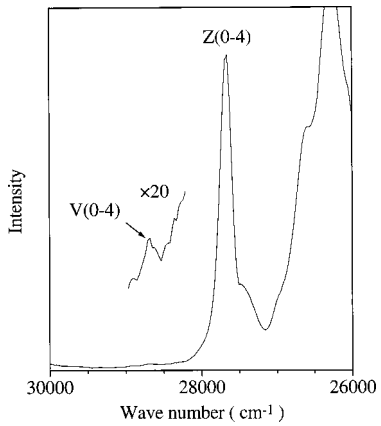


FIG. 3. Fluorescence excitation spectrum in the $^7F_0$-$^5D_4$ transition region of the $Eu^{3+}$ ion in $SiO_2$-$Na_2O$ glass at room temperature. The arrow denotes the vibronic spectrum of the $^7F_0$-$^5D_4$ transition. The lines in the lower-energy side of the $^7F_0$-$^5D_4$ zero-phonon line are assigned to the $^7F_J$-$^5G_{J'}$ zero-phonon transitions.

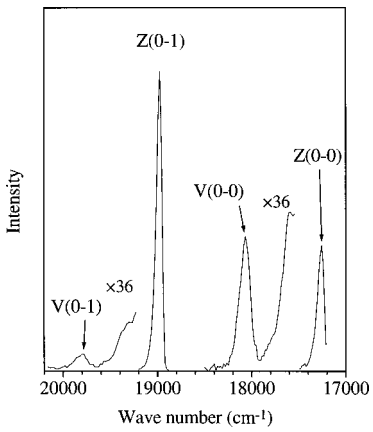


FIG. 4. Fluorescence excitation spectrum of the $Eu^{3+}$ ion in $GeO_2$-$Na_2O$ glass at 2 K.

pression for the rate of the multiphonon nonradiative transition,[4] we infer that the fluorescence from the multiplets which lie above the $^5D_2$ state in energy is also fairly weak compared with that from the $^5D_0$ state. Accordingly, we can say that the observed excitation spectra have the same strength distribution as the absorption spectra.

Table I shows the energy separations between the purely electronic lines and the peaks of the vibronic spectra associated with them. These energy separations, which correspond to the energies of the vibrations which couple with the $Eu^{3+}$ ion, are about 700, 800, 1000, and 1150 $cm^{-1}$ in

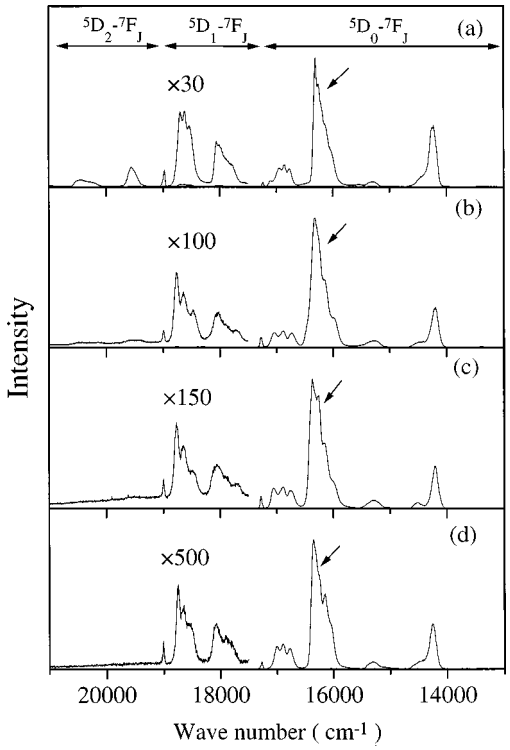


FIG. 5. Fluorescence spectra of the $Eu^{3+}$ ion doped into (a) $TeO_2$-$Na_2O$, (b) $GeO_2$-$Na_2O$, (c) $SiO_2$-$Na_2O$, and (d) $Ca(PO_3)_2$ glasses at 77 K. The arrows denote the $^5D_0$-$^7F_2$ transition. Relative intensities have been corrected for the wavelength dependence of the grating efficiency of the monochromator and the response of the photomultiplier. Intensities are normalized at the most intense peak of the $^5D_0$-$^7F_2$ transition.

TABLE I. Energy positions of the purely electronic lines (ZPL) and the peaks of the vibronic spectra (VS) in the $^7F_0$-$^5D_J$($J=0$, 1, 2, 4) and $^7F_1$-$^5D_1$ transitions of $Eu^{3+}$ in oxide glasses. Units are $cm^{-1}$.

| Sample | Transition | ZPL | VS | Separation |
|---|---|---|---|---|
| $TeO_2$- $Na_2O$ | $^7F_0$-$^5D_0$ | 17261 | unmeasured | |
| | $^7F_1$-$^5D_1$ | 18729 | 19409 | 682 |
| | $^7F_0$-$^5D_1$ | 19006 | unmeasured | |
| | $^7F_0$-$^5D_2$ | 21534 | 22263 | 729 |
| $GeO_2$-$Na_2O$ | $^7F_0$-$^5D_0$ | 17282 | 18093 | 811 |
| | $^7F_1$-$^5D_1$ | 18789 | 19618 | 829 |
| | $^7F_0$-$^5D_1$ | 19009 | 19846 | 837 |
| | $^7F_0$-$^5D_2$ | 21565 | 22403 | 838 |
| | $^7F_0$-$^5D_4$ | 27548 | 28369 | 821 |
| $SiO_2$-$Na_2O$ | $^7F_0$-$^5D_0$ | 17274 | 18287 | 1013 |
| | $^7F_1$-$^5D_1$ | 18789 | 19743 | 954 |
| | $^7F_0$-$^5D_1$ | 19000 | 20030 | 1030 |
| | $^7F_0$-$^5D_2$ | 21472 | 22488 | 1016 |
| | | 21573 | 22581 | 1008 |
| | $^7F_0$-$^5D_4$ | 27660 | 28680 | 1020 |
| $Ca(PO_3)_2$ | $^7F_0$-$^5D_0$ | 17299 | 18433 | 1134 |
| | $^7F_1$-$^5D_1$ | 18805 | 19890 | 1085 |
| | $^7F_0$-$^5D_1$ | 19034 | 20177 | 1143 |
| | $^7F_0$-$^5D_2$ | 21574 | 22708 | 1134 |

$TeO_2$-$Na_2O$, $GeO_2$-$Na_2O$, $SiO_2$-$Na_2O$, and $Ca(PO_3)_2$ glasses, respectively, for all the transitions. In the infrared measurement, an intense absorption band was observed around each energy in respective glasses without $Eu^{3+}$ ions. From these results, all the measured vibronic spectra are considered to involve the same infrared-active vibrational modes of each glass network former. These vibrational modes are assigned to the $X$-O stretching vibrations of glass forming units ($X=$P, Si, Ge, Te).[15,16] If the oscillators in the ligand molecule are not localized but a set of oscillators surrounding the rare-earth ion behave as an optical phonon, the mechanism proposed by Faulkner and Richardson rather than the cooperative transition model will be appropriate for an analysis of the vibronic spectrum involving such a phonon. However, this type of behavior is not probable in glassy materials because of the inhomogeneity of the structure.[16] Therefore, the vibronic spectra involving the intramolecular vibrations of the glass forming units should be analyzed by use of the cooperative optical transition model.

The difference of the vibrational energy among four kinds of oxide glasses explains well the fact that the relative intensities of the fluorescence from the $^5D_2$ and $^5D_1$ states to that from the $^5D_0$ state become smaller in the order of (a)–(d) of Fig. 5, because the rate of the multiphonon nonradiative relaxation, which usually describes the radiationless transition of the rare-earth ion in condensed matter, is larger for the coupling with a higher-energy vibration.[16] In the following subsections, we make quantitative analyses of the intensities of the vibronic spectra on the basis of the cooperative transition model.

TABLE II. Values of the parameters used in the calculation of the intensities of the vibronic spectra.

| |
|---|
| $\langle 4f^6[^5D]_0\|\mathbf{U}^{(2)}\|4f^6[^7F]_2\rangle^2=0.00391$ [a] |
| $\langle 4f^6[^5D]_1\|\mathbf{U}^{(2)}\|4f^6[^7F]_1\rangle^2=0.00238$ [a] |
| $\langle 4f^6[^5D]_1\|\mathbf{U}^{(2)}\|4f^6[^7F]_2\rangle^2=0.00094$ [a] |
| $\langle 4f^6[^5D]_2\|\mathbf{U}^{(2)}\|4f^6[^7F]_0\rangle^2=0.00091$ [a] |
| $\langle 4f^6[^5D]_4\|\mathbf{U}^{(4)}\|4f^6[^7F]_0\rangle^2=0.0011$ [b] |
| $\langle 4f^6[^5D]_4\|\mathbf{U}^{(2)}\|4f^6[^7F]_2\rangle^2=0.00011$ [c] |
| $\Xi(1,2)=-1.08(10^{-6}\ \mathrm{cm}^2\ \mathrm{erg}^{-1})$ [d] |
| $\Xi(3,4)=0.90(10^{-22}\ \mathrm{cm}^4\ \mathrm{erg}^{-1})$ [d] |

[a]Reference 25.
[b]Reference 26.
[c]This work.
[d]Reference 28.

### A. Vibronic spectra of the $^7F_0$-$^5D_2$ and $^7F_1$-$^5D_1$ transitions

In all the samples, the vibronic spectra of the $^7F_0$-$^5D_2$ and $^7F_1$-$^5D_1$ transitions are much stronger than those of the others. This result is explained well by the theory of Stavola and Dexter, because these two vibronic spectra are predicted by the selection rules (5) and (6) to be caused through the electric dipole-dipole interaction, which is the most dominant in the multipole-multipole expansion of the electrostatic interaction between the rare-earth ion and an oscillating ligand molecule.

The intensity of the vibronic spectrum due to the cooperative transition model is predicted by expression (1) to be proportional to the infrared oscillator strength of the intramolecular vibration. However, it is very difficult to determine this strength in our samples, because various vibrational modes in the bulk glass samples overlap in the infrared absorption spectrum. For this reason, we take the ratios of the integrated intensities among the observed vibronic spectra, so as to cancel out $|\langle g1|\mathbf{M}_m^{(1)}|g0\rangle|^2$ concerned with the above oscillator strength. The intensity ratio of the vibronic spectrum of the $^7F_1$-$^5D_1$ transition to that of the $^7F_0$-$^5D_2$ transition is calculated by using Eq. (1) as

$$\frac{V(1-1)}{V(0-2)}=\frac{1}{3}\frac{|\langle 4f^6[^5D]_1\|\mathbf{U}^{(2)}\|4f^6[^7F]_1\rangle|^2}{|\langle 4f^6[^5D]_2\|\mathbf{U}^{(2)}\|4f^6[^7F]_0\rangle|^2}\simeq 1.1. \tag{10}$$

Here, we have used the squared absolute values of the reduced matrix elements of the unit tensor operator $\mathbf{U}^{(2)}$ in Table II. Although these two vibronic transitions are allowed also through the octopole-dipole interaction, we have ignored this interaction in expression (10), because this effect is very small compared with that of the dipole-dipole interaction. We continuouly adopt this sort of approximation in the following analyses.

Table III shows the observed values of the above ratio. The experimental values in this table are corrected for the difference between the thermal populations in the $^7F_0$ state and the $^7F_1$ state. The agreement between the experimental and theoretical values is satisfactory in all the samples.

### B. Vibronic spectra of the $^7F_0$-$^5D_0$ and $^7F_0$-$^5D_1$ transitions

The purely electronic $^7F_0$-$^5D_1$ transition is the parity-allowed magnetic dipole transition, while the purely electronic $^7F_0$-$^5D_0$ line is due to the forced electric dipole transition. It has recently been proved that the dominant mechanism of the $^5D_0$-$^7F_0$ line of $Eu^{3+}$ in oxide glasses is due to the borrowing of intensity from the $^5D_0$-$^7F_2$ ($M_J=0$) transition by the $J$ mixing through the axial second-order crystal-field term $B_{20}C_{20}$.[19] Now, we investigate whether the $J$ mixing accounts for the vibronic spectra of the $^7F_0$-$^5D_0$ and $^7F_0$-$^5D_1$ transitions of the $Eu^{3+}$ ion in oxide glasses, on the basis of Eq. (9). We begin with the estimation of the values of the second-order crystal-field parameters.

TABLE III. Experimental values of $V(1-1)/V(0-2)$ and $V(0-4)/V(0-2)$, where $V(J-J')$ is the integrated intensity of the vibronic spectrum of the $^7F_J$-$^5D_{J'}$ transition.

| Sample | $V(1-1)/V(0-2)$ | $V(0-4)/V(0-2)$ |
|---|---|---|
| $TeO_2$-$Na_2O$ | $0.88\pm0.36$ | |
| $GeO_2$-$Na_2O$ | $0.96\pm0.26$ | $0.15\pm0.07$ |
| $SiO_2$-$Na_2O$ | 0.76 | $0.10\pm0.02$ |
| $Ca(PO_3)_2$ | 0.76 | |

It is known that the point symmetry of the $Eu^{3+}$ ion site in our glass samples is $C_2$, $C_{2v}$, or $C_s$. Then, the energies of the Stark levels of the $^7F_1$ manifold are expressed as

$$E(\epsilon_0)=E_0(^7F_1)+\frac{B_{20}}{5}, \tag{11a}$$

$$E(\epsilon_\pm)=E_0(^7F_1)-\frac{B_{20}}{10}\pm\frac{\sqrt{6}|B_{22}|}{10}, \tag{11b}$$

where $E_0(^7F_1)$ is the energy of the $^7F_1$ state when the second-order crystal-field component $V_c^{(2)}$ is zero. In addition, it is known that the level of $\epsilon_0$, which has the magnetic quantum number $M_J$ of zero, corresponds to the lowest-energy component in the $^7F_1$ Stark levels in our samples.[19] Therefore, the second-order crystal-field parameters $B_{20}$ and $|B_{22}|$ can be determined from the energy separations among the three $^5D_0$-$^7F_1$ fluorescence lines. In our glass samples, the crystal-field parameters have wide distributions on account of the inhomogeneity of the environment of the rare-earth ion in the host. Therefore, we regard the crystal-field parameters at the site corresponding to the peak of the purely electronic $^7F_0$-$^5D_0$ line as the representative values, and determine them from the fluorescence spectrum measured under the site-selective excitation of this peak position with a dye laser. Table IV shows the values of the second-order crystal-field parameters thus obtained. Since $|B_{22}|$ is smaller than $|B_{20}|$, we neglect the contribution of the $B_{2\pm2}C_{2\pm2}$ terms to the $J$-mixing effect in order to avoid the complexity

TABLE IV. Values of the second-order crystal-field parameters of the site corresponding to the peak of the $^7F_0$-$^5D_0$ absorption profile. Units are $cm^{-1}$.

| Sample | $B_{20}$ | $\lvert B_{22}\rvert$ |
|---|---|---|
| $GeO_2$-$Na_2O$ | $-910$ | 314 |
| $SiO_2$-$Na_2O$ | $-780$ | 269 |
| $Ca(PO_3)_2$ | $-870$ | 281 |

TABLE V. Comparison between the experimental and calculated values of $V(0-0)/V(0-2)$ and $V(0-1)/V(0-2)$.

| Sample | | Experimental | Calculated |
|---|---|---|---|
| $GeO_2$-$Na_2O$ | $V(0-0)/V(0-2)$ | $0.14\pm0.01$ | 0.04 |
| | $V(0-1)/V(0-2)$ | $0.013\pm0.001$ | 0.009 |
| $SiO_2$-$Na_2O$ | $V(0-0)/V(0-2)$ | $0.10\pm0.02$ | 0.03 |
| | $V(0-1)/V(0-2)$ | 0.012 | 0.007 |
| $Ca(PO_3)_2$ | $V(0-0)/V(0-2)$ | 0.10 | 0.03 |
| | $V(0-1)/V(0-2)$ | 0.012 | 0.008 |

due to the interference among the second-order crystal-field components. Then, the intensity ratios of the vibronic spectra of the $^7F_0$-$^5D_0$ and $^7F_0$-$^5D_1$ transitions to that of the $^7F_0$-$^5D_2$ transition are expressed using Eqs. (1) and (9), respectively, as

$$\frac{V(0-0)}{V(0-2)}=\frac{4B_{20}^2}{375\Delta_{20}^2}\frac{|\langle 4f^6[^5D]_0\|\mathbf{U}^{(2)}\|4f^6[^7F]_2\rangle|^2}{|\langle 4f^6[^5D]_2\|\mathbf{U}^{(2)}\|4f^6[^7F]_0\rangle|^2} \quad (12)$$

and

$$\frac{V(0-1)}{V(0-2)}=\frac{4B_{20}^2}{375\Delta_{20}^2}\frac{|\langle 4f^6[^5D]_1\|\mathbf{U}^{(2)}\|4f^6[^7F]_2\rangle|^2}{|\langle 4f^6[^5D]_2\|\mathbf{U}^{(2)}\|4f^6[^7F]_0\rangle|^2}. \quad (13)$$

Here, we have assumed that the transition strengths of the vibronic spectra of the $^7F_2(M_J=0)$-$^5D_0$ and $^7F_2(M_J=0)$-$^5D_1$ transitions are 1/5 of the total $^7F_2$-$^5D_0$ and $^7F_2$-$^5D_1$ vibronic transition strengths, respectively. We can calculate the intensity ratios of Eqs. (12) and (13) using $\Delta_{20}\simeq 1000$ cm$^{-1}$ and the values in Tables II and IV. In Table V, we show the comparison of these calculated intensity ratios with the experimental values determined from the excitation spectra at 2 K. The agreement between the experiments and theory is fairly good. Thus, we can say that the vibronic spectra of the $^7F_0$-$^5D_0$ and $^7F_0$-$^5D_1$ transitions appear by borrowing intensities from the vibronic spectra of the $^7F_2$-$^5D_0$ and $^7F_2$-$^5D_1$ transitions through the second-order crystal-field potential, respectively.

In our samples, the purely electronic lines due to the $^7F_0$-$^5D_1$ transition are definitely more intense than that of the $^7F_0$-$^5D_0$ transition, whereas the vibronic spectrum of the $^7F_0$-$^5D_1$ transition is apparently weaker than that of the $^7F_0$-$^5D_0$ transition. These are the properties common to most of the $Eu^{3+}$-doped materials.[29] Such a difference in intensity between the vibronic spectra of the $^7F_0$-$^5D_0$ and $^7F_0$-$^5D_1$ transitions can be explained by the difference in the magnitude of the reduced matrix elements $\langle 4f^6[^5D]_0\|\mathbf{U}^{(2)}\|4f^6[^7F]_2\rangle$ and $\langle 4f^6[^5D]_1\|\mathbf{U}^{(2)}\|4f^6[^7F]_2\rangle$, as is evident from Eqs. (12) and (13).

It is noteworthy that, in our glasses, the purely electronic line of the $^7F_0$-$^5D_1$ transition is due to the magnetic dipole transition, while the vibronic spectrum of this transition is identified as due to the electric dipole transition from the above discussion. When the Franck-Condon mechanism contributes dominantly to the vibronic spectrum, this does not occur, because the vibronic spectrum due to this mechanism has the same character as the purely electronic line.

### C. Vibronic spectrum of the $^7F_0$-$^5D_4$ transition

The $^7F_0$-$^5D_4$ vibronic transition is much weaker than the $^7F_0$-$^5D_2$ and $^7F_1$-$^5D_1$ vibronic transitions, and is comparable in intensity to the vibronic spectrum of the $^7F_0$-$^5D_0$ transition. The ratios of the integrated intensity of the vibronic spectrum of the $^7F_0$-$^5D_4$ transition to that of the $^7F_0$-$^5D_2$ transition in $GeO_2$-$Na_2O$ and $SiO_2$-$Na_2O$ glasses are shown in Table III.

If the intensity-borrowing due to the $J$ mixing between the $^7F_0$ and $^7F_2$ states mentioned in Sec. II B contributes dominantly to the $^7F_0$-$^5D_4$ vibronic transition, the above intensity ratio is calculated as

$$\frac{V(0-4)}{V(0-2)}=\frac{4B_{20}^2}{375\Delta_{20}^2}\frac{|\langle 4f^6[^5D]_4\|\mathbf{U}^{(2)}\|4f^6[^7F]_2\rangle|^2}{|\langle 4f^6[^5D]_2\|\mathbf{U}^{(2)}\|4f^6[^7F]_0\rangle|^2} \simeq 3\times10^{-4}. \quad (14)$$

Here, we have taken into account only the contribution of the axial second-order crystal-field term $B_{20}C_{20}$ for the same reason that was mentioned in Sec. V B. Since the value of $\langle 4f^6[^5D]_4\|\mathbf{U}^{(2)}\|4f^6[^7F]_2\rangle$ has not so far been reported, we have evaluated it using the wave functions of $Eu^{3+}$ calculated by Ofelt.[27] We have included only the $^7F$ and $^5D$ terms for the intermediate coupled wave function of the $^7F_2$ manifold, and only the $^7F$, $^5D$, and $^5F$ terms for the intermediate coupled wave function of the $^5D_4$ manifold, neglecting the mixing of the other $L$-$S$ coupled wave functions which make only small contributions to the above reduced matrix element.

It is clear that the observed vibronic spectra of the $^7F_0$-$^5D_4$ transition is too intense to be explained by the mixing of $^7F_2$ into $^7F_0$ even if we also take into account the borrowing of intensity through the $B_{2\pm2}C_{2\pm2}$ components. There still exists a possibility that the $J$ mixing for the $^5D_4$ state accounts for the intensity of the $^7F_0$-$^5D_4$ vibronic transition. The expression (1) predicts that, for $R\sim3$ Å, which is the approximate value of the distance between $Eu^{3+}$ and the center of the gravity of the surrounding $SiO_4$ or $GeO_4$ tetrahedra,[17,18] the $^7F_0$-$^5G_2$ vibronic spectrum is the most intense among the $^7F_0$-$^5G_{2,4,6}$ and $^5L_6$ vibronic spectra. Moreover, the absolute value of $\langle 4f^6[^5G]_2\|\mathbf{U}^{(6)}\|4f^6[^5D]_4\rangle$, which is included in the $J$-mixing coefficients between the $^5G_2$ and $^5D_4$ manifolds through the sixth-order crystal-field component $V_c^{(6)}$, is much larger than $|\langle 4f^6[^{2S+1}\Gamma]_J\|\mathbf{U}^{(\lambda)}\|4f^6[^5D]_4\rangle|$, where $([^{2S+1}\Gamma]_J=[^5G]_{4,6},[^5L]_6)$. Accordingly, the admixture of $^5G_2$ through $V_c^{(6)}$ is considered to be most important. However, we can not evaluate this contribution quantitatively, because it is not possible to determine the values of the sixth-order crystal-field parameters $B_{6q}$, which play important roles in the $J$-mixing effect in the $^5D_4$ state, on account of the overlaps of the fluorescence lines whose splittings involve $V_c^{(6)}$.

On the other hand, when the vibronic spectra of the $^7F_0$-$^5D_4$ transition are due to the octopole-dipole coupling mechanism, the above intensity ratio is estimated as

$$\frac{V(0-4)}{V(0-2)} = \frac{18}{5R^4}\frac{\Xi(3,4)^2}{\Xi(1,2)^2}\frac{|\langle 4f^6[^5D]_4\|\mathbf{U}^{(4)}\|4f^6[^7F]_0\rangle|^2}{|\langle 4f^6[^5D]_2\|\mathbf{U}^{(2)}\|4f^6[^7F]_0\rangle|^2} \simeq 0.04. \quad (15)$$

Here, we have put $R \sim 3$ Å.[17,18] Further, we have used the values of $\Xi(3,4)$ and $\Xi(1,2)$ calculated by Krupke[28] (see Table II). The calculated intensity ratio is fairly close to the experimental values obtained for the $GeO_2$-$Na_2O$ and $SiO_2$-$Na_2O$ glasses. Therefore, the $^7F_0$-$^5D_4$ vibronic transition is considered to be mostly due to the cooperative transition mechanism through the electric octopole-dipole interaction between the rare-earth ion and the oscillating glass forming unit. A part of the intensity may come from the $J$ mixing in the $^5D_4$ state.

## VI. CONCLUDING REMARKS

We have investigated the vibronic spectra of the $f$-$f$ transitions of the $Eu^{3+}$ ion in four kinds of oxide glasses of $Ca(PO_3)_2$, $SiO_2$-$Na_2O$, $GeO_2$-$Na_2O$, and $TeO_2$-$Na_2O$. These vibronic spectra involve the strongly infrared-active vibrations of the glass network formers. We have analyzed the integrated intensities of such vibronic spectra on the basis of the cooperative optical transition model of Stavola and Dexter. The results are summarized as follows.

(1) In all the four samples, the vibronic spectra of the $^7F_0$-$^5D_2$ and $^7F_1$-$^5D_1$ transitions are allowed by the electric dipole-dipole interaction between the $Eu^{3+}$ ion and the vibrating ligand molecule.

(2) The vibronic spectra of the $^7F_0$-$^5D_0$ and $^7F_0$-$^5D_1$ transitions have been found to occur by the dipole-dipole coupling through the $J$ mixing of $^7F_2$ into $^7F_0$.

(3) The vibronic spectrum of the $^7F_0$-$^5D_4$ transition has been ascribed to the cooperative transition mechanism through the electric octopole-dipole interaction and possibly also to the $J$ mixing for $^5D_4$. The contribution of $J$ mixing of $^7F_2$ into $^7F_0$ has been found to be negligibly small.

From these results, we can say that the interaction between a rare-earth ion and the nearby stretching vibrations of forming units in oxide glasses can be described well in terms of the electric multipole-multipole interaction. Thus, it will be possible to calculate the direct energy transfer rate between a rare-earth ion and a vibrating glass forming unit, and the rate of the phonon-assisted energy transfer between two rare-earth ions involving the excitation or deexcitation of the vibration of forming units, in oxide glasses, by using the calculation technique of Stavola and Dexter.[11] The rates of these processes are predicted to be small in a glass without a strong infrared-active intramolecular vibrational mode. Since these rates are often important factors that determine the properties of various optical devices, our investigation will be useful for the development of practical applications of rare-earth-doped glasses, in addition to its fundamental significance.

## ACKNOWLEDGMENTS

The authors are indebted to Dr. S. Todoroki of NTT Corporation and Professor E. Takushi of University of the Ryukyus for providing them with the glass samples used in this study.

[1] K. Suzuki, Y. Kimura, and M. Nakazawa, Appl. Phys. Lett. **55**, 2573 (1989); D. C. Hanna, R. M. Percival, R. G. Smart, and A. C. Tropper, Opt. Commun. **75**, 283 (1990).
[2] K. Hirao, S. Todoroki, D. H. Cho, and N. Soga, Opt. Lett. **18**, 1586 (1993); A. Kurita, T. Kushida, T. Izumitani, and M. Matsukawa, *ibid.* **19**, 314 (1994); M. Nogami, Y. Abe, K. Hirao, and D. H. Cho, Appl. Phys. Lett. **66**, 2952 (1995).
[3] E. M. Pacheco and C. B. de Araujo, Chem. Phys. Lett. **148**, 334 (1988); D. C. Hanna, R. M. Percival, I. R. Perry, R. G. Smart, J. E. Townsend, and A. C. Tropper, Opt. Commun. **78**, 187 (1990).
[4] See, for example, B. Henderson and G. F. Imbusch, *Optical Spectroscopy of Inorganic Solids* (Clarendon, Oxford, 1989), p. 183.
[5] S. Yatsiv, E. Ehrenfreund, and U. El-Hanany, J. Chem. Phys. **42**, 743 (1965).
[6] E. Cohen and H. W. Moos, Phys. Rev. **161**, 258 (1967).
[7] T. R. Faulkner and F. S. Richardson, Mol. Phys. **35**, 1141 (1978).
[8] T. R. Faulkner and F. S. Richardson, Mol. Phys. **36**, 193 (1978).
[9] G. Blasse, Inorg. Chim. Acta **167**, 33 (1990).
[10] G. Blasse, Inorg. Chim. Acta **169**, 25 (1990).
[11] M. Stavola and D. L. Dexter, Phys. Rev. B **20**, 1867 (1979).
[12] M. Stavola, L. Isganitis, and M. G. Sceats, J. Chem. Phys. **74**, 4228 (1981).
[13] C. de Mello Donegá and A. Meijerink, J. Lumin. **55**, 315 (1993).
[14] C. de Mello Donegá, M. J. D. Crombag, A. Meijerink, and G. Blasse, J. Lumin. **60&61**, 74 (1994).
[15] S. Todoroki, S. Tanabe, K. Hirao, and N. Soga, J. Non-Cryst. Solids **136**, 213 (1991).
[16] C. B. Layne, W. H. Lowdermilk, and M. J. Weber, Phys. Rev. B **16**, 10 (1977).
[17] R. Reisfeld and Y. Eckstein, J. Solid State Chem. **5**, 174 (1972).
[18] R. Reisfeld and N. Lieblich, J. Phys. Chem. Solids **34**, 1467 (1973).
[19] G. Nishimura and T. Kushida, Phys. Rev. B **37**, 9075 (1988); M. Tanaka, G. Nishimura, and T. Kushida, *ibid.* **49**, 16 917 (1994).
[20] M. Tanaka and T. Kushida, Phys. Rev. B **52**, 4171 (1995).
[21] M. Tanaka and T. Kushida, J. Alloys Compd. **193**, 183 (1993). The intensity ratios of the vibronic spectra of the $^7F_0$-$^5D_0$ and $^7F_0$-$^5D_1$ transitions to that of the $^7F_0$-$^5D_2$ transition in this reference should be revised as in Table V in the present paper. However, this revision does not need a change of the conclusion.
[22] M. Tanaka and T. Kushida, Chem. Phys. Lett. (to be published).
[23] B. R. Judd, Phys. Rev. **127**, 750 (1962).
[24] G. S. Ofelt, J. Chem. Phys. **37**, 511 (1962).
[25] M. J. Weber, in *Optical Properties of Ions in Crystals*, edited by H. M. Crosswhite and H. W. Moos (Interscience, New York, 1967), p. 467.
[26] W. T. Carnall, P. R. Fields, and K. Raynak, J. Chem. Phys. **49**, 4412 (1968).
[27] G. S. Ofelt, J. Chem. Phys. **38**, 2171 (1963).
[28] W. F. Krupke, Phys. Rev. **145**, 325 (1966).
[29] G. Blasse, Int. Rev. Phys. Chem. **11**, 71 (1992).